

# Rapid prototyping enzyme homologs to improve titer of nicotinamide mononucleotide using a strategy combining cell-free protein synthesis with split GFP

Qingyan Yuan<sup>1</sup>, Minhui Wu<sup>1</sup>, Yibo Liao<sup>1</sup>, Shuli Liang<sup>1</sup>, Yuan Lu<sup>2</sup>, and Ying Lin<sup>1</sup>

<sup>1</sup>South China University of Technology

<sup>2</sup>Tsinghua University

October 29, 2022

## Abstract

Engineering biological systems to test new pathway variants containing different enzyme homologs is laborious and time-consuming. To tackle this challenge, a novel strategy was developed for rapidly prototyping enzyme homologs by combining cell-free protein synthesis (CFPS) with split GFP. This strategy featured two main advantages: 1) dozens of enzyme homologs were parallelly produced by CFPS within hours, and 2) the expression level and activity of each homolog was determined [simultaneously](javascript:;) by using the split GFP assay. As a model, this strategy was applied to optimize a 3-step pathway for nicotinamide mononucleotide (NMN) synthesis. Ten enzyme homologs from different organisms were selected for each step. Here, the most productive homolog of each step was identified within 24 h rather than weeks or months. Finally, the titer of NMN was increased to 1213 mg/L by improving physiochemical conditions, tuning enzyme ratios and cofactor concentrations, and decreasing the feedback inhibition, which was a more than 12-fold improvement over the initial setup. This strategy would provide a promising way to accelerate design-build-test cycles for metabolic engineering to improve the production of desired products.

## 1 Introduction

The use of metabolic engineering to develop efficient microbial cell factories has been proved to be an attractive and powerful way to produce valuable chemicals and materials that are important for our society (Chae et al., 2017; Liu & Nielsen, 2019). However, the inherent complexity of cellular metabolism and the corresponding difficulties in balancing the trade-off between product formation and cell growth and viability have greatly slowed down the design-build-test (DBT) cycles (Nielsen & Keasling, 2016). This challenge motivates the need for new methods to accelerate the design and optimization of biosynthetic systems (Bowie et al., 2020; Bundy et al., 2018).

In recent years, cell-free systems have developed rapidly and gradually showed their strengths for speeding up DBT cycles (Dudley et al., 2015; Moore et al., 2018; Morgado et al., 2016; Sun et al., 2014). Cell-free systems are not constrained by the requirement of maintaining cellular viability and growth, thereby allowing the full allocation of carbon and energy resources to the product formation. Moreover, the openness of the cell-free systems allows direct access to the reaction conditions and cellular contents, providing great flexibility and freedom in the design and adjustment of biosynthetic reactions (Rasor et al., 2021; Vilkhovoy et al., 2020). Given the above superiorities, purified enzyme systems, which are the most common examples of cell-free biochemical synthesis, have been widely used to study enzymatic pathways and inform cellular expression (Bogorad et al., 2013; Dudley et al., 2015; Zhu et al., 2014). On the other hand, crude cell lysates have increasingly gained popularity for prototyping metabolism because they provide the endogenous metabolism for cofactor recycling and energy regeneration (Dudley et al., 2016, 2019; Jewett et al., 2008), which is

limited in purified enzyme systems. Additionally, crude lysates also have the capability to build biosynthetic pathways by expressing functional catalytic enzymes directly *in vitro* by cell-free protein synthesis (CFPS) (Dudley et al., 2020; Grubbe et al., 2020; Karim et al., 2020; Rasor et al., 2022). The hybrid approach of CFPS driving metabolic engineering (CFPS-ME) has been successfully used to prototype the synthesis of polyhydroxyalkanoate (Kelwick et al., 2018), styrene (Grubbe et al., 2020), indole alkaloids (Khatri et al., 2020), valinomycin (Zhuang et al., 2020), and acetone (Rasor et al., 2022). In addition, the Jewett group developed an elegant approach termed *in vitro* Prototyping and Rapid Optimization of Biosynthetic Enzymes (iPROBE) in the context of CFPS-ME. In iPROBE, dozens of enzyme variants in hundreds of pathway combinations were rapidly tested to improve the productivity of butanol and limonene (Dudley et al., 2020; Karim et al., 2020). To build and assess different pathway combinations, the amounts of enzyme homologs that were produced by CFPS needed to be determined by the incorporation of  $^{14}\text{C}$ -leucine in iPROBE. However, the procedure of radioactive incorporation is laborious, and radioactive  $^{14}\text{C}$ -leucine is unavailable for many laboratories. These constraints significantly limit the usefulness of iPROBE. Thus, there remains a great demand for an approach that enables testing and screening many enzyme homologs in a fast and technically simple manner.

$\beta$ -Nicotinamide mononucleotide (NMN) is a key intermediate in nicotinamide adenine dinucleotide ( $\text{NAD}^+$ ) biosynthesis and exists in all living species. NMN has been demonstrated to have effective pharmacological activities in the treatment of various diseases, such as obesity, Alzheimer’s disease, and high fat diet-induced type 2 diabetes (Poddar et al., 2019; Yoshino et al., 2011). However, the current high price of NMN hampers the widespread use and practical implementation of this molecule. While there have been many efforts to improve the production of NMN by engineering biosynthetic pathways *in vivo* (Marinescu et al., 2018; Shoji et al., 2021) or *in vitro* (Qian et al., 2022; Zhou et al., 2022), these efforts have typically explored only a small set of enzyme homologs in their optimization strategies. Hence, productive enzyme homologs and combinations for efficient synthesis of NMN are still required.

The self-complementing split GFP, engineered from superfolder green fluorescent protein (sfGFP), was first developed by Waldo and his coworkers for protein tagging (Cabantous et al., 2005). In this system, sfGFP was asymmetrically split between  $\beta$ -strands 10 and 11 into a large (GFP1–10) and a small (GFP11) fragment. The two fragments were not individually fluorescent, but they could spontaneously interact with each other to form a functional GFP. By fusing GFP11 fragment on a target protein and detecting its association with GFP1–10 fragment, this system has been used in numerous biological studies including protein solubility assays (Cabantous & Waldo, 2006), screening of enzyme mutant libraries (Santos-Aberturas et al., 2015), and imaging protein localization in living cells (Kamiyama et al., 2016; R. Tamura et al., 2021). In addition, Karim and colleagues recently showed the possibility for quantification of protein produced *in vitro* by split-GFP (Karim & Jewett, 2018). However, no one to our knowledge has yet practically applied the split GFP system to prototype enzyme homologs.

In this work, a novel strategy, which combined CFPS with split GFP, was developed for prototyping enzyme homologs (Figure 1). The key idea was that the most productive enzyme homolog for each step in the candidate pathway was rapidly identified by using a normalized screening procedure. In this procedure, enzyme homologs were produced in parallel by CFPS in a few hours, and the expression level and activity of each homolog were determined simultaneously by using the split GFP assay. As a proof of concept, the capacity of this strategy was demonstrated by optimizing a three-step pathway for synthesizing NMN. By using this strategy, the time for testing 10 enzyme homologs of each catalytic step was reduced from a few weeks to 72 hours. Additionally, NMN biosynthesis was further optimized by improving physiochemical conditions, tuning enzyme ratios and cofactor concentrations, and decreasing the feedback inhibition to reach a 12-fold improvement over our initial setup. As a result, it was expected that this strategy would accelerate the timeline of DBT cycles and enhance efforts to optimize the production of desired products in cell-free systems.

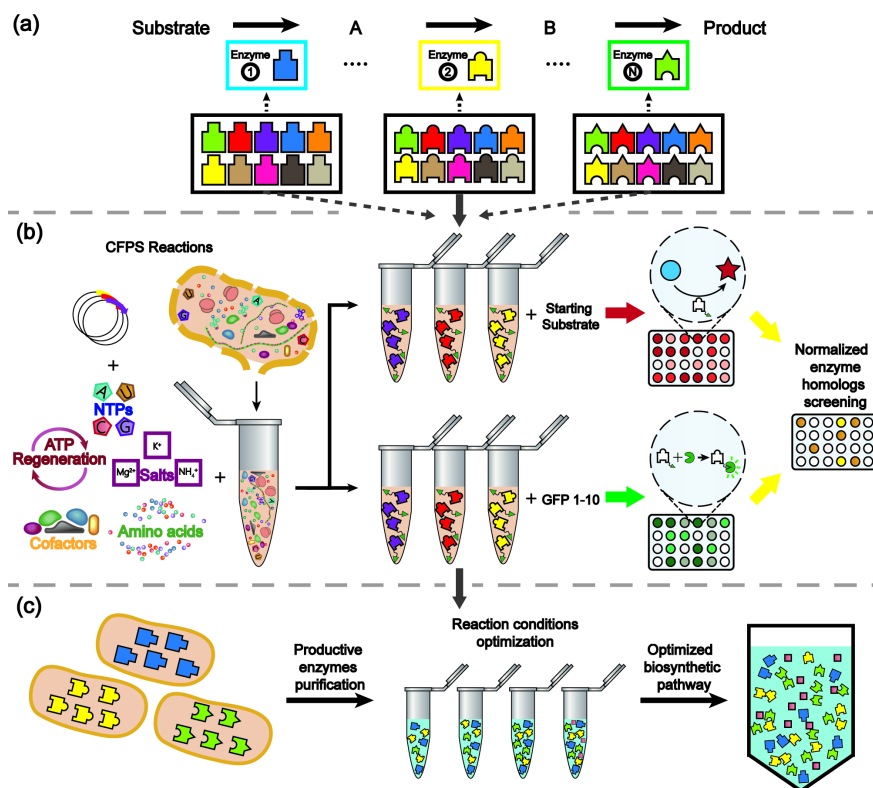


**FIGURE 1** A cell-free framework for enzyme homolog prototyping and pathway optimizing by combining cell-free protein synthesis (CFPS) with split GFP assay. (a) Biosynthetic pathways are built in a modular assembly manner. (b) Schematic representation of the strategy for the normalized screening of productive homologs. (c) Schematic representation of the workflow for building optimized biosynthetic pathway in purified enzyme systems.

## 2 Materials and methods

### 2.1 Strains and plasmids

*Escherichia coli* Top10 was used for plasmid preparation, *E. coli* BL21(DE3) was used for *in vivo* protein overexpression, and *E. coli* Rosetta(DE3) was used to prepare cell extracts for CFPS. The amino acid sequences of HsNampt (nicotinamide phosphoribosyltransferase, Nampt from *Homo sapiens*), MrNampt (Nampt from *Meiothermus ruber*), HsPrs (phosphoribosyl pyrophosphate synthetase, Prs from *Homo sapiens*), PcPrs (Prs from *Pyrobaculum calidifontis*), HsRbk (ribokinase, Rbk from *Homo sapiens*), and EcRbk (Rbk from *Escherichia coli*) were obtained from the UniProt or NCBI. To obtain additional NMN biosynthetic pathway enzyme sequences, these 6 sequences were used as query sequences to perform BLASTP search against the UniProt or NCBI database. For a particular query sequence, the resulting amino acid sequences with a percent identity value in the range of 30-99% were collected. Duplicate and incomplete sequences were discarded. The remaining sequences were aligned using ClustalW2 program (Larkin et al., 2007). The phylogenetic tree was generated using Molecular Evolutionary Genetics Analysis (MEGA 5) program (K. Tamura et al., 2011) with a Jones-Taylor-Thornton model and a maximal likelihood method. Two sequences from each phylogenetic tree constructed based on HsRbk, HsPrs or HsNampt were randomly chosen, and six sequences from each phylogenetic tree generated from EcRbk, PcPrs or MrNampt were randomly selected. Thus, there were 30 NMN pathway enzyme sequences in total. In addition, a 12-amino acid linker and a 16-amino acid “GFP11” tag were added to the end of all the 30 enzymes. To do this, the following encoded

amino acid sequence “GSDGGSGGGSTSRDHMVLHEYVNAAGIT” was added directly at the end of the coding gene sequence before the stop codon. These constructed sequences were then codon-optimized for expression in *E. coli*, synthesized, and cloned into pET-28a vector at the *Nde* I and *Xho* I sites by the synthesis company (Generay, Shanghai, China) to generate expression plasmids (Figure S1). These expression plasmids were used for both *in vivo* and *in vitro* expression of proteins.

For the preparation of the GFP1-10 fragment, the DNA fragment coding for a superfolder GFP variant with additional mutations (Cabantous & Waldo, 2006) was synthesized and cloned into pET-28a vector at the *Nde* I and *Bam*H I sites by the synthesis company (Generay, Shanghai, China) to generate plasmid pET28a-GFP1-10. To prepare pyrophosphatase from *E. coli* (EcPPase), a DNA fragment encoding EcPPase was amplified from the genomic DNA of *E. coli* BL21(DE3) using primers 5'-GGTGCCGCGCGGCAGCCATATGAGCTTACTCAACGTCCC-3' and 5'-TGGTGGTGGTGGTGGTGGTCTCGAGTTATTTATTCTTTGCGCGCT-3'. The PCR fragment was then mixed with pET28a backbone digested with the restriction enzymes *Nde* I and *Xho* I along with reagents for Gibson assembly to yield plasmid pET28a-EcPPase. All of the plasmids used in this study are listed in Table S1. Amino acid sequences of all the proteins used in this study are available in Online Supporting Information.

## 2.2 Cell extract preparation

Cell extracts were prepared using previously described methods with modifications (Karim & Jewett, 2016; Levine et al., 2019). *E. coli* Rosetta(DE3) cells were grown in 2 × YTPG media (16 g/L tryptone, 10 g/L yeast extract, 5 g/L NaCl, 7 g/L potassium phosphate monobasic, 3 g/L potassium phosphate dibasic, 18 g/L glucose). These cells were firstly cultured at the 50 mL scale in 250 mL shake flasks overnight, and then an appropriate amount of overnight culture was inoculated into 1 L of 2 × YTPG media to begin the 1 L culture at a 0.1 OD<sub>600</sub>. The inoculated 1 L culture was placed into 37 °C incubator with shaking at 200 rpm. When cells reached OD<sub>600</sub> = 0.6–0.8, the cultures were induced with 0.1 mM isopropyl-β-D-thiogalactopyranoside (IPTG). When induction cultures were grown to OD<sub>600</sub> = 3.0, the cells were harvested by centrifugation at 5,000 g at 4 °C for 10 min and were washed three times with cold S30 buffer (10 mM Tris-acetate (pH 8.2), 14 mM magnesium acetate, 60 mM potassium glutamate and 2 mM dithiothreitol (DTT)). After final wash and centrifugation, the pelleted wet cells were weighed, flash frozen in liquid nitrogen, and stored at -80 degC. To generate crude extracts, cell pellets were thawed on ice, suspended in S30 buffer (1 mL per gram cell pellet), and lysed at 20,000 psi (homogenizing pressure) using an OS Cell Disrupter (Constant Systems Limited, Northants, UK). The lysate was then centrifuged twice at 12,000 g at 4 degC for 30 min. The supernatant (i.e., lysate) was transferred to a new container without disturbing the pellet and flash-frozen in liquid nitrogen for storage at -80 degC.

## 2.3 Cell-free protein synthesis reactions

All CFPS reactions used a modified PANOX-SP formula described in previous publications with modifications (Jewett & Swartz, 2004; Levine et al., 2019). A 15 μL CFPS reaction in a 1.5 mL microcentrifuge tube was prepared by mixing the following components: ATP (1.8 mM); GTP, UTP, and CTP (1.3 mM each); folinic acid (0.1mM); oxalic acid (4 mM), *E. coli* tRNA mixture (260 μg/mL); 20 standard amino acids (2 mM each); NAD (0.4 mM); coenzyme A (0.27 mM); phosphoenolpyruvate (PEP; 33 mM); spermidine (1.5 mM); putrescine (1 mM); potassium glutamate (130 mM); magnesium glutamate (10 mM); HEPES (57 mM), and cell extract (10 μL). For each reaction plasmid was added at 4 nM. Reactions were incubated at 30 °C for 16 h.

## 2.4 Preparation of GFP1-10 detector fragment

GFP1-10 detector fragment was produced and purified from the inclusion body fraction as previously described with some modifications (Knapp et al., 2017). Briefly, *E. coli* BL21(DE3) harboring pET28a-GFP1-10 was grown in 1 L of Luria-Bertani (LB) media at 37 °C (200 rpm). Expression of GFP1-10 detector fragment was induced at OD<sub>600</sub> = 0.6 by adding of 1 mM IPTG, and cells were harvested by centrifugation after an additional 5 h of cultivation. The cell pellets were suspended in 15 mL of TNG buffer (100 mM Tris-HCl

pH 7.4, 100 mM NaCl, 10% (v/v) glycerol), lysed via pressure homogenization with one pass at 20,000 psi, and centrifuged at 12,000 g for 30 min. The supernatant was discarded and pellets were resuspended in 10 mL of TNG buffer, sonicated for 15 min and again centrifuged to sediment cell debris and inclusion bodies containing GFP1-10 detector fragment. This procedure was repeated twice. The resulting pellet, which contained mainly inclusion bodies pellet, was weighed and dissolved in 9 M urea solution (1 mL for each 75 mg of inclusion bodies). After a centrifugation step at 12,000 g for 30 min, the resulting supernatant was divided into 1 mL aliquots, and each aliquot was diluted by adding 25 mL of TNG buffer. The final GFP1–10 detector fragment solution was stored at -80 degC until use.

## 2.5 Monitoring protein production in CFPS by the split GFP assay

Unless otherwise noted, expression of GFP11 fusion enzymes in CFPS was monitored by mixing 5  $\mu$ L of sample (enzyme-enriched CFPS cell lysates) with 195  $\mu$ L of detector solution in a 96-well plate and incubation at 4 °C for 8 h to support the formation of fluorescent GFP protein. To investigate the sensitivity and accuracy of the assay, HsRbk-LG was expressed in *E. coli* BL21(DE3) and purified as described below. The purified HsRbk-LG was diluted in TNG buffer at several different concentrations between the range of 0.5  $\mu$ M and 8  $\mu$ M. 5  $\mu$ L of the respective HsRbk-LG dilution was mixed with 195  $\mu$ L of detector solution in a 96-well plate. Once both solutions were mixed, the 96-well plate was stored at 4 °C, and the fluorescence signals were measured at different time points. In all cases, fluorescence was measured in the microplate reader (Infinite M200, Tecan Austria GmbH) with the wavelength of excitation at 488 nm and emission at 520 nm. The complementation fluorescence ([?]F) was calculated using Equation (1) described in Online Supporting Information.

## 2.6 Protein in vivo expression and purification

The plasmids used to express the desired enzyme genes were transformed into *E. coli* BL21(DE3) by the chemical thermal shock method. Single colonies were picked from agar plates containing 50  $\mu$ g/mL kanamycin and then were inoculated into 10 mL of LB medium containing the same antibiotic to produce the first culture. The first culture was incubated at 37 °C in a shaker at 200 rpm overnight for 13-16 h. The appropriate amount of overnight culture was inoculated into LB media containing the same antibiotic to begin the 100 mL culture at a 0.1 OD<sub>600</sub>. The inoculated 100 mL culture was grown under the same culture conditions. When the OD<sub>600</sub> reached 0.6-0.8, enzyme expression was induced by adding 0.2 mM IPTG and the culture was then incubated at 16 degC and 180 rpm for 16 h. The cells were collected by centrifugation at 5,000 g at room temperature for 10 min and were washed two times with binding buffer (20 mM Tris-HCl, 0.1 M NaCl, pH 7.5). After final wash and centrifugation, the pelleted wet cells were suspended in 10 mL of binding buffer and disrupted by sonication. The lysate was then centrifuged at 10,000 g and 4 degC for 30 min, and the supernatant, which contained the crude protein, was loaded onto a Ni-NTA His-Bind Resin. The protein was eluted with elution buffer (20 mM Tris-HCl, 0.1 M NaCl, 0.25 M imidazole, pH 8.0), and then the desired protein was collected. The protein concentration was measured with the Bio-Rad Bradford protein kit with bovine serum albumin (BSA) as the standard.

## 2.7 NMN synthesis in CFPS-ME reactions and purified enzyme system reactions

All NMN synthesis reactions were carried out at a volume of 100  $\mu$ L in 96-well plates. To produce NMN in CFPS-ME reactions, NMN pathway enzymes were expressed in CFPS reactions as described in Section 2.3. When CFPS reactions were complete, the enzyme-enriched CFPS cell lysates were mixed with desired substrates and cofactors to activate NMN synthesis. “Blank” CFPS reactions with no DNA added were used as control. See Table S2 for a more detailed description of the reaction components. To produce NMN in purified enzyme system reactions, purified NMN pathway enzymes were obtained as described in Section 2.6 and then mixed with desired substrates and cofactors to activate NMN synthesis. See Table S3 for a more detailed description of the reaction conditions. Unless otherwise noted, NMN synthesis reactions were incubated at 40 °C for 3 h. After reactions were finished, the concentrations of NMN in samples were analyzed immediately.

## 2.8 NMN measurement

The concentrations of NMN in samples were analyzed using a validated fluorometric assay method with some modifications (Marinescu et al., 2018; Shoji et al., 2021; Zhang et al., 2011). Assays were performed in 96-well plates with a 90  $\mu$ L final volume per well, consisting of 25  $\mu$ L of sample, 10  $\mu$ L of 20% (v/v) acetophenone in dimethyl sulfoxide (DMSO), and 10  $\mu$ L of 2 M KOH. The mixture was incubated on ice for 2 min before adding 45  $\mu$ L of 88% formic acid to each well. After incubation at 37 °C for 10 min, 60  $\mu$ L of the mixture in each well was transferred into a flat-bottom 96-well black plate. The fluorescence was measured on a microplate reader (Infinite M200, Tecan Austria GmbH) with the following settings: excitation wavelength 382nm and emission wavelength 445nm. The concentration of NMN was calculated from the fluorometric assay standard curve (Figure S2), which was created from the fluorescence data of standard NMN (Sigma N3501-25MG) samples in series concentrations.

### 3 Results and discussion

#### 3.1 Design of NMN biosynthetic pathways

In cells, NMN is an intermediate in NAD<sup>+</sup> biosynthesis produced from nicotinamide (NAM) and phosphoribosyl pyrophosphate (PRPP) by nicotinamide phosphoribosyltransferase (Nampt, EC 2.4.2.12) (Lin et al., 2016; Poddar et al., 2019). However, the direct use of PRPP as a substrate for NMN preparation is not acceptable because it is not only expensive but also unstable (Hove-Jensen et al., 2017). To avoid this problem, three possible NMN biosynthesis pathways were designed, in which adenosine, adenosine monophosphate (AMP), or ribose was used as the starting material to generate PRPP, respectively (Figure 2a). In pathway I, adenosine was first converted to AMP by the catalysis of adenosine kinase (Adk, EC 2.7.2.10), and then PRPP and adenine were synthesized through AMP and pyrophosphate (PPi), which was catalyzed by adenine phosphoribosyltransferase (Apt, EC 2.4.2.7). In pathway II, the conversion of adenosine into AMP was omitted, and PRPP was directly generated from AMP and PPi. In pathway III, ribose was converted into PRPP through two catalytic steps. First, ribokinase (Rbk, EC 2.7.1.15) catalyzed the phosphorylation of ribose using ATP as a donor of the phosphate group to generate ribose-5-phosphate (R5P). Second, R5P was pyrophosphorylated by ATP to form PRPP catalyzed by phosphoribosyl pyrophosphate synthetase (Prs, EC 2.7.6.1). The last step for all three pathways was the same. In this step, the synthesized PRPP reacted with NAM to form NMN and by-product PPi, which was catalyzed by Nampt.

After designing three possible biosynthetic pathways for NMN production, we next aimed to verify the feasibility of these pathways. As the thermodynamic analysis was a straightforward and reliable way to determine whether a metabolic reaction or pathway was feasible or not (Flamholz et al., 2012), the standard Gibbs free energy changes ( $\Delta_r G^\circ$ ) for the three pathways were calculated by using the eQuilibrator website (equilibrator.weizmann.ac.il/) at pH 8.0 and 0.05 M of ionic strength. The  $\Delta_r G^\circ$  of pathways I, II, and III was -4.2 kJ/mol, +11.8 kJ/mol, and -45.7 kJ/mol, respectively (Figure 2b). Although Apt could convert AMP to generate PRPP in one step, the  $\Delta_r G^\circ$  of this step is +26.3 kJ/mol, which means that this reaction is difficult to occur. On the other hand, the  $\Delta_r G^\circ$  of all the three steps in pathway III was negative, indicating that the overall reaction of this pathway was thermodynamically favorable. Therefore, the pathway I and II containing Apt were discarded, and the most thermodynamically favorable pathway III with ribose as the co-substrate together with NAM was selected as a promising route for NMN synthesis.

We next investigated the capacity of this pathway for producing NMN experimentally. Two homologs for each reaction step were selected as initial enzyme sets. They were Rbk from *Escherichia coli* (Maj & Gupta, 2001) and *Homo sapiens* (Park et al., 2007), Prs from *Pyrobaculum calidifontis* (Bibi et al., 2016) and *Homo sapiens* (Nosal et al., 1993), and Nampt from *Meiothermus ruber* and *Homo sapiens* (Hara et al., 2011). All enzymes were expressed in *Escherichia coli* BL21(DE3) and purified using a Ni-NTA affinity column. By combining different enzyme homologs, each possible combination was constructed using 1  $\mu$ M of each enzyme (8 unique pathway combinations), and the performance in the synthesis of NMN of each pathway combination was tested. NMN was successfully detected in all 8 pathway combinations (Figure 2c), which strongly suggested that pathway III is feasible for producing NMN. The NMN titers produced by these initial enzyme sets ranged from 12 mg/L to 101 mg/L, and the two highest NMN titers were obtained from the pathway combinations in which both Prs and Nampt are from prokaryotic organisms (that is, Prs from

*Pyrobaculum calidifontis* and Nampt from *Meiothermus ruber*). This result not only implied that prokaryotic enzymes are more likely to be productive for NMN synthesis but also highlighted the importance of testing enzyme homologs to enhance pathway performance.

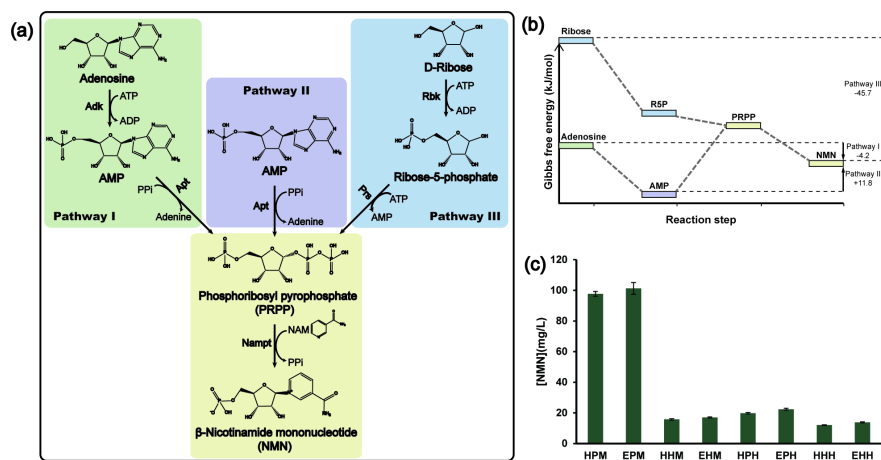


**FIGURE 2** Design and selection of NMN biosynthetic pathways. (a) Design of three pathways for NMN biosynthesis. (b) Standard Gibbs free energy changes for NMN biosynthesis pathways. (c) Using 8 pathway combinations to produce NMN. HPM, HsRbk + PcPrs + MrNampt; EPM, EcRbk + PcPrs + MrNampt; HHM, HsRbk + HsPrs + MrNampt; EHM, EcRbk + HsPrs + MrNampt; HPH, HsRbk + PcPrs + HsNampt; EPH, EcRbk + PcPrs + HsNampt; HHH, HsRbk + HsPrs + HsNampt; EHH, EcRbk + HsPrs + HsNampt. See Table S2 for details. Error bars represent the standard deviation of three biological replicates. Adk, adenosine kinase; Apt, adenine phosphoribosyltransferase; Rbk, ribokinase; Prs, phosphoribosyl pyrophosphate synthetase; Nampt, nicotinamide phosphoribosyltransferase. PPI, pyrophosphate.

### 3.2 Adaptation of split GFP assay to monitor protein expression in CFPS

The protein production of CFPS was usually monitored and quantified by using radioactive amino acid incorporation (Jewett & Swartz, 2004; Karim & Jewett, 2018), which allowed researchers to control and assess pathway performance in a precise manner in the CFPS-ME framework (Grubbe et al., 2020; Karim et al., 2020; Rasor et al., 2022). However, radioactive incorporation was unavailable for many laboratories and its procedure was laborious. To overcome the limitations of radioactive incorporation, we adapted a split GFP assay to monitor CFPS protein production. In brief, a 12-amino acid linker and a 16-amino acid GFP-derived peptide tag (GFP11) were cloned to the C terminus of the gene encoding the target protein. The fusion protein was produced via CFPS, while a truncated, non-fluorescing detector GFP protein (GFP1-10) was produced separately. Combining the CFPS cell lysates which contained the GFP11-tagged protein with the detector for a short time would elicit a quantifiable fluorescent signal. Hence, protein production of CFPS could be monitored simply by fluorescence determination (Figure 3a).

As a proof-of-principle, the split GFP assay was applied to monitor the expression levels of 6 enzymes included in the initial enzyme sets for NMN synthesis. An 84 nucleotide sequence encoding the 12-amino acid linker and 16-amino acid “GFP11” tag was added directly at the end of the coding sequence of Hs/MrNampt, Hs/PcPrs, and Hs/EcRbk before the stop codon. The constructed sequences were cloned into the pET-28a vector at the *Nde* I and *Xho* I sites (Figure S1) by the synthesis company. CFPS reactions were performed by using these enzyme expression plasmids as DNA templates and incubated for 16 h at 30°C. When the CFPS reactions were complete, the enzyme-enriched CFPS cell lysates were mixed and incubated with a GFP1-10 detector solution. Compared to the “Blank” CFPS reaction (using water instead of expression template), a combination of six enzyme-enriched cell lysates and the GFP1-10 detector all emitted significant fluorescence as expected. More importantly, the fluorescence was directly proportional to the amount of added enzyme-

enriched cell lysates (Figure 3b). To further assess the sensitivity and accuracy of the assay, serial dilutions of purified GFP11-tagged HsRbk (HsRbk-LG) were prepared, and each dilution was then added to the GFP1-10 detector solution to regenerate GFP fluorescence. As shown in Figure 3c, there always was a strong correlation ( $R^2 > 0.99$ ) between the complementation fluorescence and the amount of HsRbk at different incubation time points (ranging from 8 to 16h). In addition, the amount of detected protein could reach the picomolar level, which indicated that this approach was highly sensitive and accurate. Taken together, these results suggested that the split GFP assay allowed to monitor protein expression in CFPS in a convenient and sensitive way.

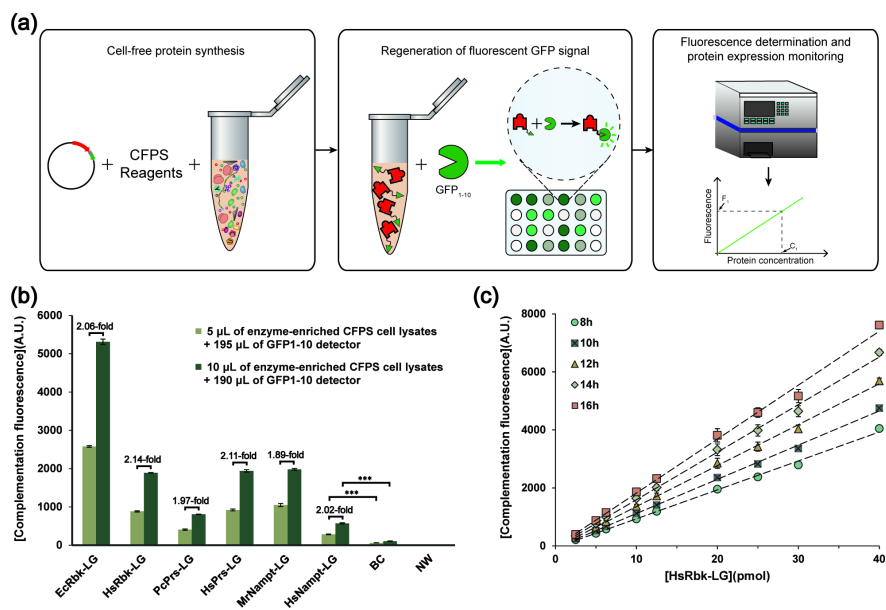


**FIGURE 3** Monitoring protein production in CFPS by the split GFP assay. (a) Schematic representation of the workflow for monitoring protein production in CFPS by the split GFP assay. (b) Producing six NMN pathway enzymes by CFPS and monitoring their expression levels by the split GFP assay. BC: Blank CFPS reaction; NW: Nanopure water. Statistical significance was examined using a two-tailed T-test analysis. \*\*\*:  $P < 0.001$ . Error bars represent the standard deviation of three biological replicates. (c) Sensitivity of the split GFP assay. The correlation coefficients between complementation fluorescence value and the amount of HsRbk-LG were 0.9986, 0.9991, 0.9992, 0.9987, and 0.9977 for incubating for a period of 8 h, 10 h, 12 h, 14 h, and 16 h, respectively. Error bars represent the standard deviation of three biological replicates.

### 3.3 Prototyping enzyme homologs for NMN biosynthesis by using a normalized screening procedure

After designing a feasible biosynthetic pathway for NMN production and demonstrating the ability to monitor CFPS via split GFP assay, a normalized screening procedure, which incorporated these two technologies, was employed to rapidly prototype enzyme homologs (Figure 1b). Briefly, enzyme homologs were parallelly expressed by CFPS. For each homolog, its CFPS reaction mixture was divided into two parts: one part was used to catalyze the conversion of the desired substrate to product, and the other part was mixed with GFP 1-10 detector to regenerate the fluorescent GFP signal for monitoring its expression level. The ratio ( $R_{T/F}$ ) between the final titer of the product and the fluorescence value was calculated for each individual homolog. Then the normalized screening was performed by comparing the  $R_{T/F}$  values based on a criterion, in which the homolog with the highest  $R_{T/F}$  value was regarded as the most productive homolog.

To identify the putative enzyme homologs in NMN biosynthetic pathway, the amino acid sequences of

HsNampt, MrNampt, HsPrs, PcPrs, HsRbk and EcRbk were used as query sequences to perform BLAST analysis against the Universal Protein Resource (UniProt) or National Center for Biotechnology Information database (NCBI) database. For a particular query sequence, some resulting fallacious sequences were discarded, and then the left sequences were used to generate a phylogenetic tree. Thus, six phylogenetic trees were obtained in total (Figure 4). Notably, since the prokaryotic NMN pathway enzymes were found more likely to be productive (Figure 3c), we had a bias to select more sequences from the phylogenetic trees that were constructed based on the enzymes from prokaryotes (i.e., EcRbk, PcPrs and MrNampt). As a result, two sequences from each phylogenetic tree constructed based on HsRbk (Figure 4a), HsPrs (Figure 4c), or HsNampt (Figure 4e), and six sequences from each phylogenetic tree generated from EcRbk (Figure 4b), PcPrs (Figure 4d), or MrNampt (Figure 4f) were selected. In summary, there were 10 homologs for each enzyme of the three-enzyme NMN pathway, which included two query homologs and eight homologs chosen from phylogenetic trees. The 30 enzyme sequences were all cloned into the pET28a-derived expression plasmid (Figure S1) for adding the linker and GFP11 tag.

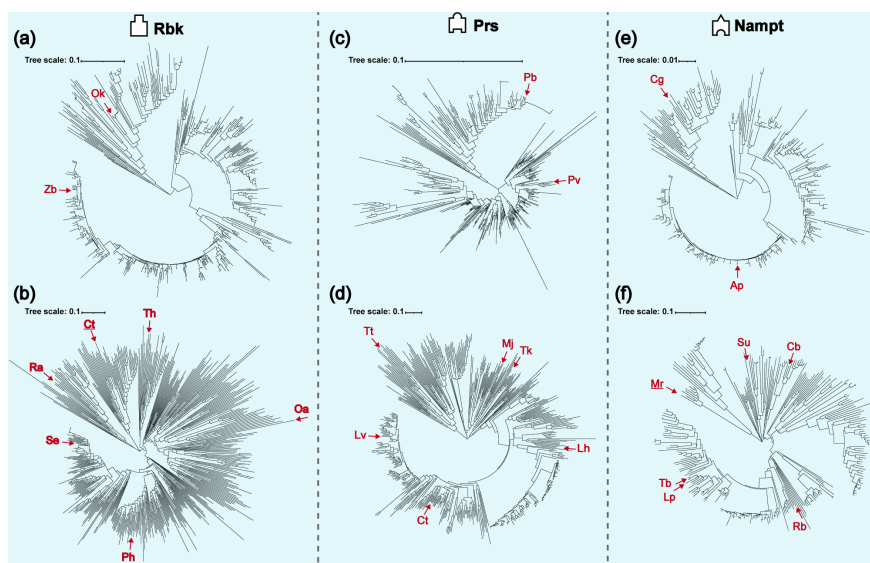


**FIGURE 4** Phylogenetic comparison of enzyme sequences to select diverse enzyme homologs for testing. Scale bars denote substitutions per site. (a), (b), (c), (d), (e), and (f) represent the phylogenetic tree which was constructed based on HsRbk, EcRbk, HsPrs, PcPrs, HsNampt, and MrNampt, respectively. Zb, *Zosterops borbonicus*; Ok, *Oncorhynchus kisutch*; Ct, *Clostridium taeniosporum*; Th, *Thermoflexus hugenholtzii* JAD2; Oa, *Ornatilinea apprima*; Ph, *Photobacterium halotolerans*; Se, *Superficieibacter electus*; Ra, *Ralstonia* sp. A12; Pb, *Pogonomyrma barbatus*; Pv, *Pogona vitticeps*; Tt, *Tepidiphilus thermophilus*; Tk, *Thermococcus kodakarensis*; Mj, *Methanocaldococcus jannaschii*; Lh, *Limimonas halophila*; Ct, *Clostridium thermobutyricum*; Lv, *Lactobacillus vaccinostrercus* DSM 20634; Ap, *Aptenodytes patagonicus*; Cg, *Cottoperca gobio*; Mr, *Meiothermus rufus*; Su, *Sulfurovum* sp. FS06-10; Cb, *Comamonadaceae bacterium*; Rb, *Rhodocyclaceae bacterium*; Tb, *Thermomonas brevis*; Lp, *Lysobacter prati*. Visualizations of trees were generated using the Interactive Tree of Life tool (<https://itol.embl.de/>).

After obtaining the NMN biosynthetic pathway enzymes library, the most productive enzyme homolog for each step was rapidly identified by applying the normalized screening procedure in a step-by-step manner. At first, 10 candidate homologs of Nampt were evaluated using the normalized screening. The complementation GFP fluorescence showed that the expression of LpNampt, CgNampt, and ApNampt via CFPS was poor (Figure 5b). In our experience, the complementation fluorescence ([?]F) value below 200 implied that the amount of corresponding protein expressed in CFPS was not able to activate pathway reaction successfully, so

these homologs were ruled out from calculating  $R_{T/F}$  values. By comparing the  $R_{T/F}$  values of the remaining seven homologs, it was found that the  $R_{T/F}$  value of SuNampt was the highest. Next, the candidate homologs of Prs were characterized through the normalized screening procedure by assembling with SuNampt. MjPrs was picked out because it had the highest  $R_{T/F}$  value (Figure 5c). At last, OkRbk was identified as the most productive Rbk homolog by combining with SuNampt and MjPrs in the normalized screening (Figure 5d). By using the normalized screening procedure, the best performing enzyme homolog of each step was identified from 10 different enzyme variants in 24 h (i.e., a 16-hour CFPS reaction step for expressing enzyme homologs and a 8-hour assay step for the determination of the expression level and activity of each homolog). However, it would take several weeks if 10 enzymes were tested *in vivo* due to the constraints of cell growth and laborious genetic manipulations (Nielsen & Keasling, 2016; Wu et al., 2016). In addition, Santos and colleagues recently reported the development of a method for screening of enzyme mutant libraries, which also utilized the split GFP system (Santos-Aberturas et al., 2015). However, the enzyme mutants were expressed using the cell-based approach in this method, which meant that the time-consuming cloning, cell culturing, and lysing processes were still needed, thus limiting the screening speed and throughput of this method. By contrast, our normalized screening procedure could be expanded easily into a high-speed and high-throughput format because the enzyme homologs could be readily obtained from the efficient CFPS reactions.

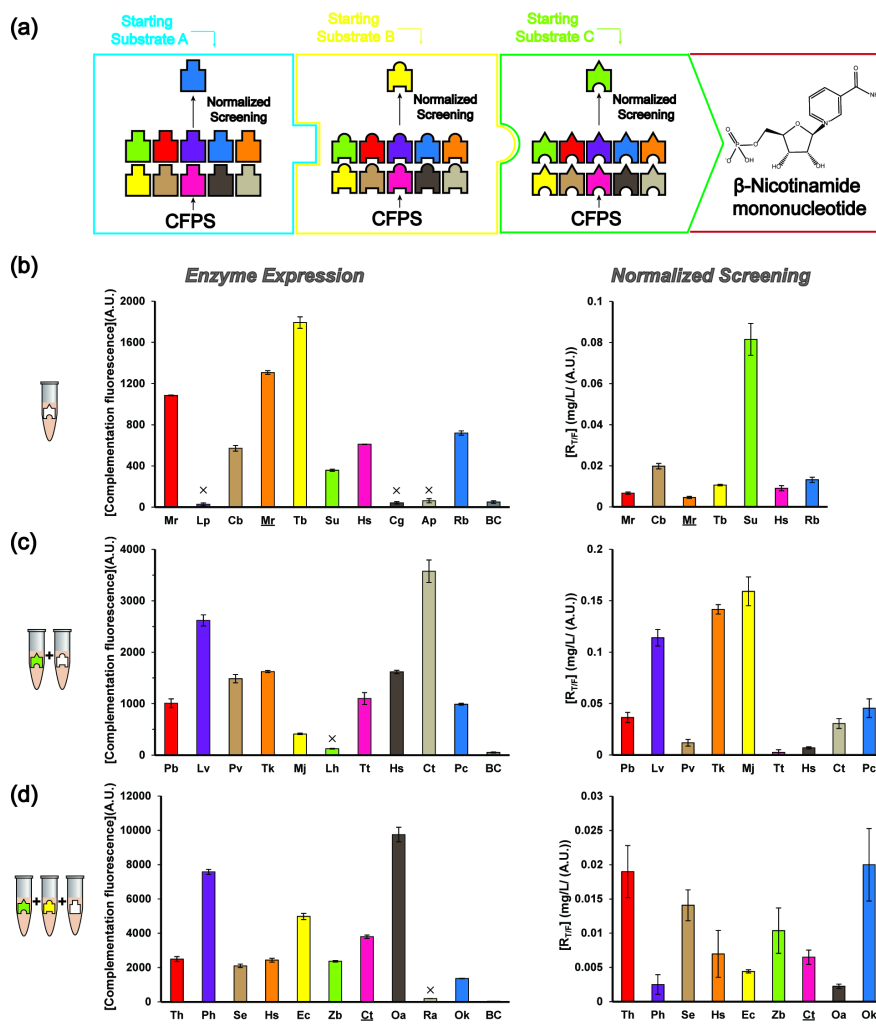


**FIGURE 5** Identifying the most productive enzyme homolog for each step in a step-wise manner by using the normalized screening. (a) Schematic representation of the workflow for step-wise identifying the most productive enzyme homologs. (b) The most active Nampt homolog, SuNampt, was first identified. “Mr” represents Nampt from *Meiothermus ruber*, and “Mr” represents Nampt from *Meiothermus rufus*. (c) By mixing with SuNampt, the most productive Prs homolog was proved to be MjPrs. (d) By combining with SuNampt and Mjprsr, the most active Rbk homolog (i.e., OkRbk) was identified. The left histograms in (b), (c), and (d) show the results of the complementation fluorescence values for Nampt homologs, Prs homologs, and Rbk homologs, respectively. Error bars represent the standard deviation of three biological replicates. The (×) symbols represent that the  $R_{T/F}$  values of these homologs were not calculated. The right histograms in (b), (c), and (d) show the results of  $R_{T/F}$  values of different NMN metabolic pathway enzymes. Error bars represent propagated error. See Table S2 for more detailed information on NMN synthesis reactions.

### 3.4 Testing and optimizing NMN biosynthesis

To confirm the results obtained using the normalized screening procedure, the 30 homologs were expressed in *E. coli* BL21(DE3), purified (Figure S4), and tested for their activities of NMN biosynthesis. It was noticed that the performance of our normalized screening procedure in evaluating the homologs with middle activity, such as CbNampt, PcPrs, and ThRbk, was unsatisfactory. However, there was no occurrence of the false positives using this procedure. As shown in Figure 6, the activity of SuNampt, MjPrs, and OkRbk was highest in the respective reaction system. In addition, the combination of OkRbk, MjPrs, and SuNampt improved NMN production by 2.9-fold to 295 mg/L from the best initial enzyme set, which consisted of EcRbk, PcPrs and MrNampt (Figure 2c). These results indicated that the normalized screening procedure provided a quick and easy way to screen active enzyme homologs. Particularly, it was well suitable for preliminary screening of dozens of enzyme homologs to find candidate homologs with high catalytic activities.

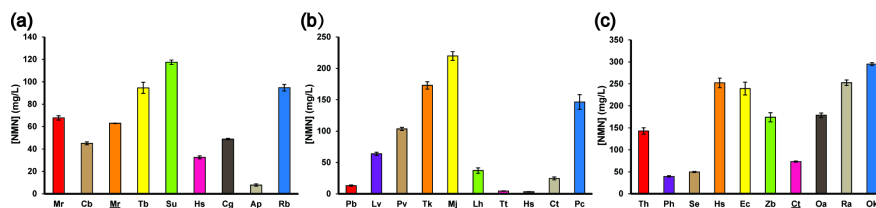


**FIGURE 6** NMN titers produced by different Nampt (a), Prs (b), and Rbk (c) homologs. Error bars represent the standard deviation of three biological replicates. See Table S3 for more detailed information on NMN synthesis reactions.

With the most productive enzyme homologs in hand, we next stepped through a series of optimizations to activate their full potential for NMN biosynthesis. To obtain the optimal reaction conditions, the effects of temperature, pH, enzyme ratios,  $Mg^{2+}$ , and ATP concentrations on NMN production were estimated. The influence of different temperatures on NMN production was investigated at 25-45 °C for 3 h. The highest titer of NMN was obtained at 40 °C (Figure 7a). The influence of pH (6.0-9.0) on NMN production was determined at 40 degC for 3 h. As shown in Figure 7b, the highest titer of NMN was obtained at pH 8.0. Then the effect of enzyme ratios was explored. The optimal enzyme ratios of SuNampt, MjPrs, and OkRbk were found to be 0.5:1:1 (Figure 7c). Then, response surface methodology was carried out to optimize the concentrations of  $Mg^{2+}$  and ATP. 10 mM  $Mg^{2+}$  and 16 mM ATP were determined to be optimal (Table S4). After the above optimizations, the NMN titer was improved to 433 mg/L (Figure 7d, Table S4), with a yield of 64.8% (Figure S5a).

As the yield of NMN was satisfactory, we stopped optimizing the reaction conditions and then sought to determine if the NMN production could be further improved when doubling the concentrations of substrates and enzymes simultaneously. Unfortunately, it was found that increasing substrates and enzymes concentrations led to a notable decrease in yield of NMN, while the NMN titer increased slightly (Figure S5a). Combined with the results in Figure 7c, which indicated that increasing the ratio of SuNampt excessively

was deleterious to NMN production, we therefore speculated that the decreased yield was possibly due to the feedback inhibition caused by PPi, which was the byproduct of Nampt-catalyzed reaction and thus would be rapidly accumulated when the amount of SuNampt was increased. The openness of the cell-free systems allowed us to examine this hypothesis and adjust the NMN biosynthetic reaction in a fast and facile manner. First, an extra 0.5 mM PPi was directly added to the NMN synthesis reaction. As expected, a further decrease in the NMN yield was observed (Figure S5b), indicating that PPi indeed has the inhibitory effects on NMN production. This result was well consistent with a recent study that suggested that PPi has feedback inhibition on Nampt (Ngivprom et al., 2022). Next, we tested whether the NMN production could be improved by removing the PPi inhibition. To do this, we took advantage of the convenient nature of CFPS to express the pyrophosphate-hydrolyzing enzyme, pyrophosphatase (EC 3.6.1.1) from *E. coli* (EcPPase) and then added it to the NMN synthesis reaction. In comparison to the control reaction, the addition of EcPPase produced by CFPS significantly improved the NMN production; the yield of NMN was increased from 41.3% to 64.1% (Figure S5b). Taken together, these results suggested that there is an inhibition effect of PPi on NMN production and decreasing this feedback inhibition is beneficial for NMN biosynthesis. Finally, EcPPase was expressed in *E. coli* and purified, and then its concentration was finely tuned for the highest NMN production. The results showed that the optimal concentration of EcPPase was 0.5  $\mu$ M (Figure S6), and under this condition, the final titer of NMN was increased to 1213 mg/L, with a yield of 90.8% (Figure 7d, Figure S6), which was a more than 12-fold improvement of NMN titer over the initial setup (Figure 2c).

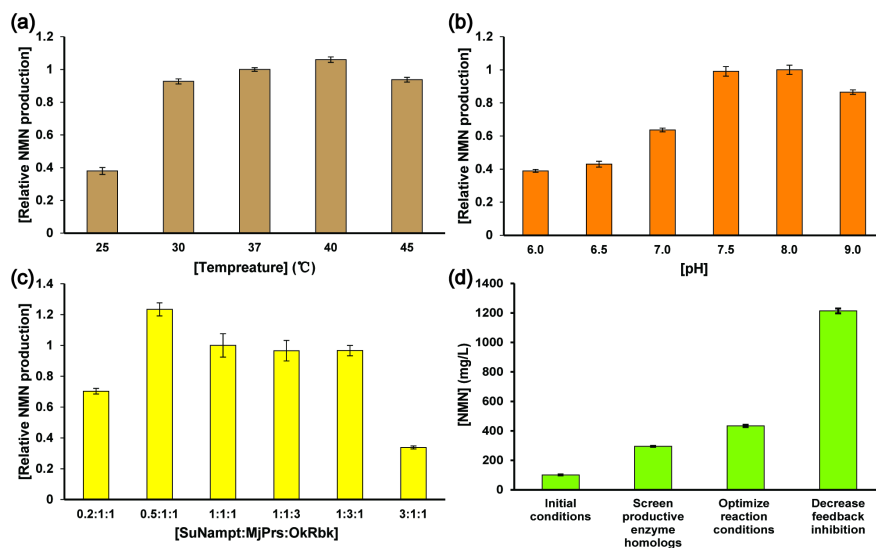


**FIGURE 7** Optimization of NMN production. Effects of temperature from 25-45°C (a), pH from 6.0-9.0 (b), and enzyme ratios (c) on NMN production. (d) NMN synthesis was improved by stepping through a series of optimizations. Error bars represent the standard deviation of three biological replicates. See Table S3 for more detailed information on NMN synthesis reactions.

#### 4 Conclusion

In this work, a novel strategy that combined CFPS with split GFP for rapidly prototyping enzyme homologs was developed. To demonstrate the potential of this strategy, it was applied to optimize a three-step biosynthetic pathway for the production of NMN. By applying this strategy, the time to characterize 10 enzyme homologs of each catalytic step had been reduced from a few weeks to 24 hours. Finally, the three-step NMN biosynthetic pathway was further optimized to reach a 12-fold improvement over our initial setup.

A key feature of our work was that the expression of pathway enzymes in CFPS was monitored by using the split GFP assay instead of  $^{14}$ C-leucine incorporation, relative to previous works which applied CFPS-ME

approach to prototype biosynthetic pathways (Dudley et al., 2020; Grubbe et al., 2020; Karim et al., 2020; Karim & Jewett, 2016; Rasor et al., 2022). Compared with  $^{14}\text{C}$ -leucine incorporation, the split GFP assay provided a fast and technically simple way to monitor proteins produced by CFPS in a time as fast as 2 h (Figure S2). In addition, the split GFP signal correlated well ( $R^2 > 0.99$ ) (Figure 3c) with the amount of GFP11-tagged proteins, and the amount of protein to be detected could reach the picomolar level (Figure 3c) (Cabantous et al., 2005). Another important feature of our work was that the high activity enzyme homologs were identified using a normalized screening procedure. In this procedure, the enzyme homologs were rapidly produced by CFPS in parallel, and then these proteins were mixed with essential substrates and GFP 1-10 detector fragment to perform target molecule production and protein content quantification, respectively. At last, the most productive enzyme homolog could be easily selected by choosing the homolog with the highest  $R_{T/F}$  value. This normalized screening procedure offers a rapid and facile way for characterizing enzyme homologs, especially for the primary screening of a large amount of enzyme homologs to identify potential enzyme hits. Taken together, it is anticipated that the strategy combining CFPS with split GFP will facilitate rapid design-build-test cycles for identifying the most productive enzyme homologs to produce desired products. In addition, this strategy is expected to expand the application space and reduce the application difficulty of CFPS-ME, which has been proved to be a powerful strategy for prototyping the synthesis of high-value commodity chemicals.

## ACKNOWLEDGMENTS

This study was supported by the National Key R&D Program of China (No. 2018YFA0901700) and the National Natural Science Foundation of China (No. 31871739).

## CONFLICT OF INTERESTS

The authors declare that they have no conflict of interests.

## AUTHOR CONTRIBUTIONS

Qingyan Yuan and Ying Lin designed the research; Qingyan Yuan, Minhui Wu, and Yibo Liao performed the experiments; Ying Lin, Yuan Lu, and Shuli Liang provided guidance and experience; Qingyan Yuan analyzed the data; Qingyan Yuan and Ying Lin wrote the manuscript; Ying Lin, Yuan Lu, and Shuli Liang discussed the results and contributed to improvement of the manuscript. All authors read and approved the final manuscript.

## DATA AVAILABILITY STATEMENT

The data that support the findings of this study are available from the corresponding author upon reasonable request.

## References

- Bibi, T., Perveen, S., Aziz, I., Bashir, Q., Rashid, N., Imanaka, T., & Akhtar, M. (2016). Pcal\_1127, a highly stable and efficient ribose-5-phosphate pyrophosphokinase from *Pyrobaculum calidifontis*. *Extremophiles*, *20* (6), 821–830. <https://doi.org/10.1007/s00792-016-0869-z>
- Bogorad, I. W., Lin, T.-S., & Liao, J. C. (2013). Synthetic non-oxidative glycolysis enables complete carbon conservation. *Nature*, *502* (7473), 693–697. <https://doi.org/10.1038/nature12575>
- Bowie, J. U., Sherkhanov, S., Korman, T. P., Valliere, M. A., Opgenorth, P. H., & Liu, H. (2020). Synthetic Biochemistry: The Bio-inspired Cell-Free Approach to Commodity Chemical Production. *Trends in Biotechnology*, *38* (7), 766–778. <https://doi.org/10.1016/j.tibtech.2019.12.024>
- Bundy, B. C., Hunt, J. P., Jewett, M. C., Swartz, J. R., Wood, D. W., Frey, D. D., & Rao, G. (2018). Cell-free biomanufacturing. *Current Opinion in Chemical Engineering*, *22*, 177–183. <https://doi.org/10.1016/j.coche.2018.10.003>

- Cabantous, S., Terwilliger, T. C., & Waldo, G. S. (2005). Protein tagging and detection with engineered self-assembling fragments of green fluorescent protein. *Nature Biotechnology* , 23 (1), 102–107. <https://doi.org/10.1038/nbt1044>
- Cabantous, S., & Waldo, G. S. (2006). In vivo and in vitro protein solubility assays using split GFP. *Nature Methods* , 3 (10), 845–854. <https://doi.org/10.1038/nmeth932>
- Chae, T. U., Choi, S. Y., Kim, J. W., Ko, Y.-S., & Lee, S. Y. (2017). Recent advances in systems metabolic engineering tools and strategies. *Current Opinion in Biotechnology* , 47 , 67–82. <https://doi.org/10.1016/j.copbio.2017.06.007>
- Dudley, Q. M., Anderson, K. C., & Jewett, M. C. (2016). Cell-Free Mixing of Escherichia coli Crude Extracts to Prototype and Rationally Engineer High-Titer Mevalonate Synthesis. *ACS Synthetic Biology* , 5 (12), 1578–1588. <https://doi.org/10.1021/acssynbio.6b00154>
- Dudley, Q. M., Karim, A. S., & Jewett, M. C. (2015). Cell-free metabolic engineering: Biomanufacturing beyond the cell. *Biotechnology Journal* , 10 (1), 69–82. <https://doi.org/10.1002/biot.201400330>
- Dudley, Q. M., Karim, A. S., Nash, C. J., & Jewett, M. C. (2020). In vitro prototyping of limonene biosynthesis using cell-free protein synthesis. *Metabolic Engineering* , 61 , 251–260. <https://doi.org/10.1016/j.ymben.2020.05.006>
- Dudley, Q. M., Nash, C. J., & Jewett, M. C. (2019). Cell-free biosynthesis of limonene using enzyme-enriched Escherichia coli lysates. *Synthetic Biology* , 4 (1), 1–9. <https://doi.org/10.1093/synbio/ysz003>
- Flamholz, A., Noor, E., Bar-Even, A., & Milo, R. (2012). eQuilibrator—the biochemical thermodynamics calculator. *Nucleic Acids Research* , 40 (D1), D770–D775. <https://doi.org/10.1093/nar/gkr874>
- Grubbe, W. S., Rasor, B. J., Kruger, A., Jewett, M. C., & Karim, A. S. (2020). Cell-free styrene biosynthesis at high titers. *Metabolic Engineering* , 61 , 89–95. <https://doi.org/10.1016/j.ymben.2020.05.009>
- Hara, N., Yamada, K., Shibata, T., Osago, H., & Tsuchiya, M. (2011). Nicotinamide Phosphoribosyltransferase/Visfatin Does Not Catalyze Nicotinamide Mononucleotide Formation in Blood Plasma. *PLoS ONE* , 6 (8), e22781. <https://doi.org/10.1371/journal.pone.0022781>
- Hove-Jensen, B., Andersen, K. R., Kilstrup, M., Martinussen, J., Switzer, R. L., & Willemoes, M. (2017). Phosphoribosyl Diphosphate (PRPP): Biosynthesis, Enzymology, Utilization, and Metabolic Significance. *Microbiology and Molecular Biology Reviews* , 81 (1), e00040–e00016. <https://doi.org/10.1128/MMBR.00040-16>
- Jewett, M. C., Calhoun, K. A., Voloshin, A., Wu, J. J., & Swartz, J. R. (2008). An integrated cell-free metabolic platform for protein production and synthetic biology. *Molecular Systems Biology* , 4 (1), 220. <https://doi.org/10.1038/msb.2008.57>
- Jewett, M. C., & Swartz, J. R. (2004). Mimicking the Escherichia coli cytoplasmic environment activates long-lived and efficient cell-free protein synthesis. *Biotechnology and Bioengineering* , 86 (1), 19–26. <https://doi.org/10.1002/bit.20026>
- Kamiyama, D., Sekine, S., Barsi-Rhyne, B., Hu, J., Chen, B., Gilbert, L. A., Ishikawa, H., Leonetti, M. D., Marshall, W. F., Weissman, J. S., & Huang, B. (2016). Versatile protein tagging in cells with split fluorescent protein. *Nature Communications* , 7 (1), 11046. <https://doi.org/10.1038/ncomms11046>
- Karim, A. S., Dudley, Q. M., Juminaga, A., Yuan, Y., Crowe, S. A., Heggstad, J. T., Garg, S., Abdalla, T., Grubbe, W. S., Rasor, B. J., Coar, D. N., Torculas, M., Krein, M., Liew, F. M. (Eric), Quattlebaum, A., Jensen, R. O., Stuart, J. A., Simpson, S. D., Kopke, M., & Jewett, M. C. (2020). In vitro prototyping and rapid optimization of biosynthetic enzymes for cell design. *Nature Chemical Biology* , 16 (8), 912–919. <https://doi.org/10.1038/s41589-020-0559-0>

- Karim, A. S., & Jewett, M. C. (2016). A cell-free framework for rapid biosynthetic pathway prototyping and enzyme discovery. *Metabolic Engineering* , 36 , 116–126. <https://doi.org/10.1016/j.ymben.2016.03.002>
- Karim, A. S., & Jewett, M. C. (2018). Cell-Free Synthetic Biology for Pathway Prototyping. In *Methods in Enzymology* (pp. 31–57). <https://doi.org/10.1016/bs.mie.2018.04.029>
- Kelwick, R., Ricci, L., Chee, S. M., Bell, D., Webb, A. J., & Freemont, P. S. (2018). Cell-free prototyping strategies for enhancing the sustainable production of polyhydroxyalkanoates bioplastics. *Synthetic Biology* , 3 (1), 1–12. <https://doi.org/10.1093/synbio/ysy016>
- Khatri, Y., Hohlman, R. M., Mendoza, J., Li, S., Lowell, A. N., Asahara, H., & Sherman, D. H. (2020). Multicomponent Microscale Biosynthesis of Unnatural Cyanobacterial Indole Alkaloids. *ACS Synthetic Biology* , 9 (6), 1349–1360. <https://doi.org/10.1021/acssynbio.0c00038>
- Knapp, A., Rippahn, M., Volkenborn, K., Skoczinski, P., & Jaeger, K.-E. (2017). Activity-independent screening of secreted proteins using split GFP. *Journal of Biotechnology* , 258 , 110–116. <https://doi.org/10.1016/j.jbiotec.2017.05.024>
- Larkin, M. A., Blackshields, G., Brown, N. P., Chenna, R., McGettigan, P. A., McWilliam, H., Valentin, F., Wallace, I. M., Wilm, A., Lopez, R., Thompson, J. D., Gibson, T. J., & Higgins, D. G. (2007). Clustal W and Clustal X version 2.0. *Bioinformatics* , 23 (21), 2947–2948. <https://doi.org/10.1093/bioinformatics/btm404>
- Levine, M. Z., Gregorio, N. E., Jewett, M. C., Watts, K. R., & Oza, J. P. (2019). Escherichia coli-Based Cell-Free Protein Synthesis: Protocols for a robust, flexible, and accessible platform technology. *Journal of Visualized Experiments* , 144 , 1–11. <https://doi.org/10.3791/58882>
- Lin, J. B., Kubota, S., Ban, N., Yoshida, M., Santeford, A., Sene, A., Nakamura, R., Zapata, N., Kubota, M., Tsubota, K., Yoshino, J., Imai, S., & Apte, R. S. (2016). NAMPT-Mediated NAD<sup>+</sup> Biosynthesis Is Essential for Vision In Mice. *Cell Reports* , 17 (1), 69–85. <https://doi.org/10.1016/j.celrep.2016.08.073>
- Liu, Y., & Nielsen, J. (2019). Recent trends in metabolic engineering of microbial chemical factories. *Current Opinion in Biotechnology* , 60 , 188–197. <https://doi.org/10.1016/j.copbio.2019.05.010>
- Maj, M. C., & Gupta, R. S. (2001). The effect of inorganic phosphate on the activity of bacterial ribokinase. *Journal of Protein Chemistry* , 20 (2), 139–144. <https://doi.org/10.1023/A:1011081508171>
- Marinescu, G. C., Popescu, R.-G., Stoian, G., & Dinischiotu, A. (2018).  $\beta$ -nicotinamide mononucleotide (NMN) production in Escherichia coli. *Scientific Reports* , 8 (1), 12278. <https://doi.org/10.1038/s41598-018-30792-0>
- Moore, S. J., MacDonald, J. T., Wienecke, S., Ishwarbhai, A., Tsipa, A., Aw, R., Kylilis, N., Bell, D. J., McClymont, D. W., Jensen, K., Polizzi, K. M., Biedendieck, R., & Freemont, P. S. (2018). Rapid acquisition and model-based analysis of cell-free transcription–translation reactions from nonmodel bacteria. *Proceedings of the National Academy of Sciences* , 115 (19), E4340–E4349. <https://doi.org/10.1073/pnas.1715806115>
- Morgado, G., Gerngross, D., Roberts, T. M., & Panke, S. (2016). *Synthetic Biology for Cell-Free Biosynthesis: Fundamentals of Designing Novel In Vitro Multi-Enzyme Reaction Networks* (pp. 117–146). [https://doi.org/10.1007/10\\_2016\\_13](https://doi.org/10.1007/10_2016_13)
- Ngivprom, U., Lasin, P., Khunnonkwao, P., Worakaensai, S., Jantama, K., Kamkaew, A., & Lai, R. (2022). Synthesis of Nicotinamide Mononucleotide from Xylose via Coupling Engineered Escherichia coli and a Biocatalytic Cascade. *ChemBioChem* , 23 (11). <https://doi.org/10.1002/cbic.202200071>
- Nielsen, J., & Keasling, J. D. (2016). Engineering Cellular Metabolism. *Cell* , 164 (6), 1185–1197. <https://doi.org/10.1016/j.cell.2016.02.004>
- Nosal, J. M., Switzer, R. L., & Becker, M. A. (1993). Overexpression, purification, and characterization of recombinant human 5-phosphoribosyl-1-pyrophosphate synthetase isozymes I and II. *Journal of Biological Chemistry* , 268 (14), 10168–10175. [https://doi.org/10.1016/S0021-9258\(18\)82187-1](https://doi.org/10.1016/S0021-9258(18)82187-1)

- Park, J., van Koeverden, P., Singh, B., & Gupta, R. S. (2007). Identification and characterization of human ribokinase and comparison of its properties with E. coli ribokinase and human adenosine kinase. *FEBS Letters* , 581 (17), 3211–3216. <https://doi.org/10.1016/j.febslet.2007.06.009>
- Poddar, S. K., Sifat, A. E., Haque, S., Nahid, N. A., Chowdhury, S., & Mehedi, I. (2019). Nicotinamide Mononucleotide: Exploration of Diverse Therapeutic Applications of a Potential Molecule. *Biomolecules* ,9 (1), 34. <https://doi.org/10.3390/biom9010034>
- Qian, X.-L., Dai, Y.-S., Li, C.-X., Pan, J., Xu, J.-H., & Mu, B. (2022). Enzymatic synthesis of high-titer nicotinamide mononucleotide with a new nicotinamide riboside kinase and an efficient ATP regeneration system. *Bioresources and Bioprocessing* , 9 (1), 26. <https://doi.org/10.1186/s40643-022-00514-6>
- Rasor, B. J., Vögeli, B., Jewett, M. C., & Karim, A. S. (2022). *Cell-Free Protein Synthesis for High-Throughput Biosynthetic Pathway Prototyping* (Vol. 2433, pp. 199–215). [https://doi.org/10.1007/978-1-0716-1998-8\\_12](https://doi.org/10.1007/978-1-0716-1998-8_12)
- Rasor, B. J., Vögeli, B., Landwehr, G. M., Bogart, J. W., Karim, A. S., & Jewett, M. C. (2021). Toward sustainable, cell-free biomanufacturing. *Current Opinion in Biotechnology* , 69 , 136–144. <https://doi.org/10.1016/j.copbio.2020.12.012>
- Santos-Aberturas, J., Dörr, M., Waldo, G. S., & Bornscheuer, U. T. (2015). In-Depth High-Throughput Screening of Protein Engineering Libraries by Split-GFP Direct Crude Cell Extract Data Normalization. *Chemistry & Biology* , 22 (10), 1406–1414. <https://doi.org/10.1016/j.chembiol.2015.08.014>
- Shoji, S., Yamaji, T., Makino, H., Ishii, J., & Kondo, A. (2021). Metabolic design for selective production of nicotinamide mononucleotide from glucose and nicotinamide. *Metabolic Engineering* , 65 , 167–177. <https://doi.org/10.1016/j.ymben.2020.11.008>
- Sun, Z. Z., Yeung, E., Hayes, C. A., Noireaux, V., & Murray, R. M. (2014). Linear DNA for Rapid Prototyping of Synthetic Biological Circuits in an Escherichia coli Based TX-TL Cell-Free System. *ACS Synthetic Biology* , 3 (6), 387–397. <https://doi.org/10.1021/sb400131a>
- Tamura, K., Peterson, D., Peterson, N., Stecher, G., Nei, M., & Kumar, S. (2011). MEGA5: Molecular Evolutionary Genetics Analysis Using Maximum Likelihood, Evolutionary Distance, and Maximum Parsimony Methods. *Molecular Biology and Evolution* , 28 (10), 2731–2739. <https://doi.org/10.1093/molbev/msr121>
- Tamura, R., Jiang, F., Xie, J., & Kamiyama, D. (2021). Multiplexed labeling of cellular proteins with split fluorescent protein tags. *Communications Biology* , 4 (1), 1–8. <https://doi.org/10.1038/s42003-021-01780-4>
- Vilkhovoy, M., Adhikari, A., Vadhin, S., & Varner, J. D. (2020). The Evolution of Cell Free Biomanufacturing. *Processes* , 8 (6), 675. <https://doi.org/10.3390/pr8060675>
- Wu, G., Yan, Q., Jones, J. A., Tang, Y. J., Fong, S. S., & Koffas, M. A. G. (2016). Metabolic Burden: Cornerstones in Synthetic Biology and Metabolic Engineering Applications. *Trends in Biotechnology* ,34 (8), 652–664. <https://doi.org/10.1016/j.tibtech.2016.02.010>
- Yoshino, J., Mills, K. F., Yoon, M. J., & Imai, S. (2011). Nicotinamide Mononucleotide, a Key NAD+ Intermediate, Treats the Pathophysiology of Diet- and Age-Induced Diabetes in Mice. *Cell Metabolism* ,14 (4), 528–536. <https://doi.org/10.1016/j.cmet.2011.08.014>
- Zhang, R. Y., Qin, Y., Lv, X. Q., Wang, P., Xu, T. Y., Zhang, L., & Miao, C. Y. (2011). A fluorometric assay for high-throughput screening targeting nicotinamide phosphoribosyltransferase. *Analytical Biochemistry* , 412 (1), 18–25. <https://doi.org/10.1016/j.ab.2010.12.035>
- Zhou, C., Feng, J., Wang, J., Hao, N., Wang, X., & Chen, K. (2022). Design of an in vitro multienzyme cascade system for the biosynthesis of nicotinamide mononucleotide . *Catalysis Science & Technology* ,12 (4), 1080–1091. <https://doi.org/10.1039/d1cy01798e>

Zhu, F., Zhong, X., Hu, M., Lu, L., Deng, Z., & Liu, T. (2014). In vitro reconstitution of mevalonate pathway and targeted engineering of farnesene overproduction in *Escherichia coli*. *Biotechnology and Bioengineering* , 111 (7), 1396–1405. <https://doi.org/10.1002/bit.25198>

Zhuang, L., Huang, S., Liu, W. Q., Karim, A. S., Jewett, M. C., & Li, J. (2020). Total in vitro biosynthesis of the nonribosomal macrolactone peptide valinomycin. *Metabolic Engineering* , 60 , 37–44. <https://doi.org/10.1016/j.ymben.2020.03.009>